JOURNAL OF SOLID STATE CHEMISTRY 64, 81–89 (1986)

Rutile Phases in the $CrNbO_4$–VO_2–MoO_2 System: Preparation and Properties

C. J. CHEN, M. GREENBLATT* AND K. RAVINDRAN NAIR†

Department of Chemistry, Rutgers, The State University of New Jersey, New Brunswick, New Jersey 08903

AND J. V. WASZCZAK

AT&T Bell Laboratories, Murray Hill, New Jersey 07974

Received July 31, 1985; in revised form January 1, 1986

A wide domain of solid solutions have been prepared in the $CrNbO_4$–VO_2–MoO_2 system with rutile-type structure. Electrical conductivity (77–300 K) and magnetic susceptibility (4.2–300 K) measurements of the samples show small band gap semiconducting behavior with very low activation energies ($E_a < kT$) and strong magnetic interactions of the metal ions, respectively. The magnitude of electrical conductivity and magnetic interactions increases with increasing Mo content. The transport properties are discussed in terms of the structural and electronic properties of the compounds. Results of lithium insertion reactions on selected compounds are also presented. © 1986 Academic Press, Inc.

Introduction

A number of metal dioxides, particularly those of the transition metals, adopt rutile or rutile-related structures. There have been numerous studies, both experimental and theoretical, attempting to correlate the electronic and structural properties of these phases (*1–3*). The binary transition metal dioxides of V, Nb, Mo, W, and Re have incompletely filled *d* shells and the variation of the observed structural and physical properties are associated with the number of unpaired d electrons (*1–7*). In addition to their interesting structural, electrical, and magnetic properties, some of these oxides have been investigated for potential applications in the photoelectrolysis of water (*8–11*) and as possible cathode materials for high energy density secondary batteries (*12*).

The ideal rutile structure may be described as a hexagonal close-packed oxygen lattice with octahedrally coordinated metal ions forming edge-shared infinite chains along the [001] direction of the tetragonal unit cell ($P4_2/mnm$); the chains are cross-linked by octahedra sharing corners to form an equal number of identical vacant channels. Strong cation–cation interactions often occur between metal ions across edge-sharing octahedra, resulting in anomalously short metal–metal distances and/or structural modification of the rutile type

* To whom correspondence should be addressed.

† Present address: Regional Research Laboratory, Trivandrum 695019, India.

0022-4596/86 $3.00

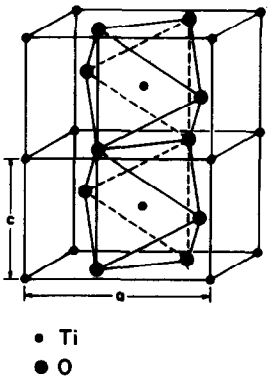

FIG. 1. The rutile structure, showing closest metal–metal interactions along the [001] direction.

(VO_2 at $T < 340$ K, MoO_2, for example). Figure 1 shows that this metal–metal interaction occurs along the c direction and that the metal–metal distance is equal to the length of the c axis of the undistorted rutile unit cell. In VO_2 ($T < 340$ K), MoO_2, WO_2, and ReO_2 very short metal–metal distances have been observed, indicating the presence of single and multiple metal–metal bonds, respectively (*3*).

For example, rutile-type metallic VO_2 in which the V–V distances are equivalent (2.87 Å) undergoes a phase transition at 340 K to a monoclinic, low-temperature semiconducting polymorph in which there are alternating short (2.65 Å) and long (3.12 Å) V–V distances along the c axis (*4*). Similarly, MoO_2 is metallic, but monoclinic and there are alternating short and long metal–metal interactions in the c direction (*13*). There is a close relationship between the magnitude of the short metal–metal distances and the number of unpaired d electrons which are not engaged in metal–oxygen bonding and are available for metal–metal bonding (*4–6*). It has been found that the axial ratio c/a of the rutile-related oxides is a good measure of the short metal–metal distance and may be used as a comparison of the rutile structures consisting of metal ions of different sizes (*3–6*). Studies of ternary rutile phases of the type $Cr_{1-x}Mo_xO_2$, $V_{1-x}Mo_xO_2$, and $Nb_{1-x}Mo_xO_2$ show that the rutile structure is stabilized with incorporation of Mo and that the unit cell volume increases as expected from ionic size while the magnitude of the c axis decreases with increasing Mo content, probably due to the increased Mo–Mo interaction along that direction (*5*).

The band model energy diagram proposed by Goodenough (*14*) and modified by Rogers *et al.* (*3*) which qualitatively accounts for the structural and electronic properties of rutile-related dioxides has been confirmed to be basically correct by recent X-ray photoemission (XPS) studies (*15–17*).

Recently we have reported on quarternary rutile-type oxides $CrVNbO_6$, $FeVNbO_6$, $NiV_2Nb_2O_{10}$, $Cr_2V_2WO_{10}$, and $Cr_2Nb_2WO_{10}$ (*18–21*), each with the general formula MO_2. It was shown that these compounds adopt the ideal rutile structure, can form grossly nonstoichiometric phases with retention of this structure, are semiconducting, and their electronic and magnetic properties may be correlated with the number of unpaired d electrons introduced into the rutile network.

In an attempt to prepare new quarternary rutile type molybdates, compounds of $M'_xM''_yMoO_{2+2(x+y)}$ with M' = first row transition metal and M'' = V, Nb, Mo, and W were systematically studied. Only a few compositions produced single rutile phases—$NiNb_2MoO_8$ and Cr_2WMoO_8, for example. In the $CrNbO_4$–$yMoO_2$ system we found that the rutile structure is adopted only when $y < 0.3$. However, the solubility of MoO_2 in $CrNbO_4$ can be increased with the simultaneous incorporation of VO_2 to form a series of solid solutions $CrNbO_4$–xVO_2–$yMoO_2$. The analogous system of $FeNbO_4$–xVO_2–$yMoO_2$ with selected compositions was also studied for comparison. We found that the electrical conductivity and activation energy change systematically with composition in these series of

compounds, so that a close control of the electronic properties for specific applications may be achieved by careful adjustment of the chemical composition. Possible application of these mixed oxides as cathode materials in secondary lithium batteries was also investigated. The results of the physicochemical investigations of the new mixed transition metal rutile phases in the system $CrNbO_4$–xVO_2–$yMoO_2$ are presented in this paper.

Experimental

High-purity (>99.99%) oxides, Cr_2O_3, Nb_2O_5, Fe_2O_3, V_2O_5, and MoO_3 (Johnson Matthey, Inc.), were used as starting materials. VO_2 was prepared by heating a stoichiometric mixture of V_2O_5 and V metal powder in evacuated and sealed quartz tubes at 700°C for 40 hr. MoO_2 was prepared by heating a mixture of MoO_3 and Mo metal in a similar manner. All compounds in the system $CrNbO_4$–xVO_2–$yMoO_2$ were prepared from stoichiometric mixtures of Cr_2O_3, Nb_2O_5, VO_2, and MoO_2. Reactant oxides were intimately ground and mixed in an agate mortar and then pelletized at 20,000 psi. The pellets were sealed in quartz tubes at 2.5×10^{-2} torr and heated at 1000–1100°C for 7 to 12 days. When necessary the materials were reground and refired several times until well crystallized single phases were obtained.

The identity and purity of the phases prepared were monitored by X-ray powder diffraction patterns which were recorded on a Philips Norelco diffractometer with filtered copper radiation. Silicon powder was used as an internal standard. Patterns were recorded in the range $10° \leq 2\theta \leq 70°$ and scanned with a speed of $\frac{1}{2}$ 2θ/min. The lattice parameters were obtained by least-square fits of the observed powder diffraction data for all the materials.

For the electrical resistivity measurements the pelletized samples in each case were sintered at 1000°C in evacuated quartz tubes for 7 days. The electrical resistivities were measured using the van der Pauw (*22*) method. Contacts were made by painting Englehard No. 16 silver paint on the sample disks; their ohmic behavior was established by measuring their current-voltage characteristics. There was no change in the measured resistivities when a disk was cut to half its original thickness. Magnetic susceptibility data were obtained by the Faraday method as described previously (*23*).

Lithium insertion reactions of selected rutile phases were carried out with *n*-butyllithium (*n*-BuLi) in hexane. Electrochemical lithium insertion was carried out for selected phases in a small test cell using the rutile phase mixed with 20% graphite as cathode, Li metal foil as anode and 1 *M* $LiClO_4$ in propylene carbonate (PC) as electrolyte.

Results and Discussions

The following subsystems with the rutile structure have been identified: I, $CrNbV_xO_{4+2x}$ with $0 \leq x \leq 6$; II, $CrNbMo_yO_{4+2y}$ with $0 \leq y < 0.3$; III, $CrNbV_{0.5}Mo_yO_{5+2y}$ with $0 \leq y < 2$; IV, $CrNbVMo_yO_{6+2y}$, $0 \leq y < 3$; and V, $CrNbV_2Mo_yO_{8+2y}$, $0 \leq y < 5$. The X-ray powder diffraction patterns of all products were consistent with a tetragonal unit cell of the rutile type (space group $P4_2/mnm$). In no case were additional lines observed in the diffraction pattern leading to the conclusion that the metal ions do not order.

The variation of lattice parameters as a function of x for subsystem I ($CrNbV_xO_{4+2x}$) is shown in Fig. 2. Both the a and c axes are seen to decrease with increasing x in accordance with the substitution of the smaller V^{4+} cations for Cr^{3+} and Nb^{5+} (*24*). The variation of lattice parameters as a function of y is shown in Fig. 3 for subsystems II, III, and V. The increase of the a axis with increasing Mo content (y)

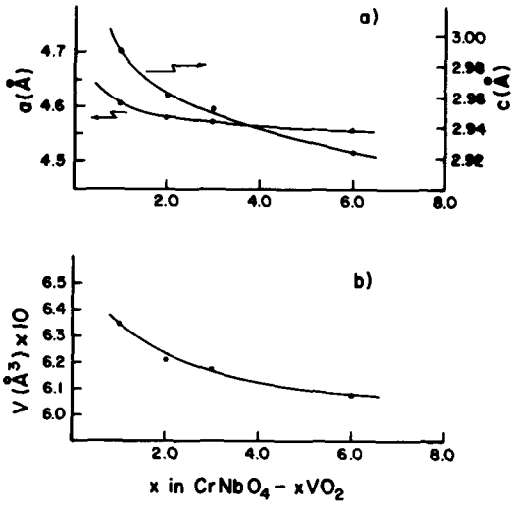

FIG. 2. Variation of (a) the lattice parameters a and c and (b) the volume of the unit cell as a function of VO_2 content in $CrNbO_4$–xVO_2 rutile phases.

(Fig. 3a) is accompanied by a simultaneous shortening of the c axis (Fig. 3b). The break in the trend of decreasing c seen at $CrNbV_2Mo_2O_{12}$ suggests increased metal–metal interactions beyond $y > 2$ (Fig. 3b). Similar trends are found in the system, $FeNbO_4$–$2VO_2$–$yMoO_2$ (subsystem VI, the upper limit is $y = 6$; beyond this composition the X-ray powder diffraction pattern shows multiphase composition) for which the variation of lattice parameters is included in Fig. 3. It is noteworthy that in the Fe system, more molybdenum can be incorporated than in the Cr system of identical composition, i.e., $FeNbV_2Mo_6O_{20}$ vs $CrNbV_2Mo_4O_{16}$. The decrease in the c axis is indicative of increased bonding interactions between neighboring metal ions in edge-sharing octahedra as discussed above. Moreover, such interactions are apparently much weaker in the $CrNbO_4$–VO_2 (or $FeNbO_4$–VO_2) systems but increase with increasing Mo content in the corresponding $CrNbO_4$–xVO_2–$yMoO_2$ (and $FeNbO_4$–$2VO_2$–$yMoO_2$) systems.

The relationship between short metal–metal distances along the c axis and the number of d electrons available for metal–metal interaction in rutile has already been discussed (*1–7*). In the pseudo-ternary phases studied here it is more appropriate to look at the c/a trends with increasing VO_2 and/or MoO_2 content. Table I shows that in the $CrNbO_4$–xVO_2 phases c/a decreases very slowly with increasing x suggesting that the electrons are localized on V^{4+} and that there is little metal–metal interaction either by direct $t_{2g}(d)$ or by indirect $t_{2g}(d)$-$\pi(p)$ overlap. In contrast, the axial ratio decreases dramatically with increasing MoO_2 content for the $CrNbO_4$–xVO_2–$yMoO_2$ compounds in each case (Ta-

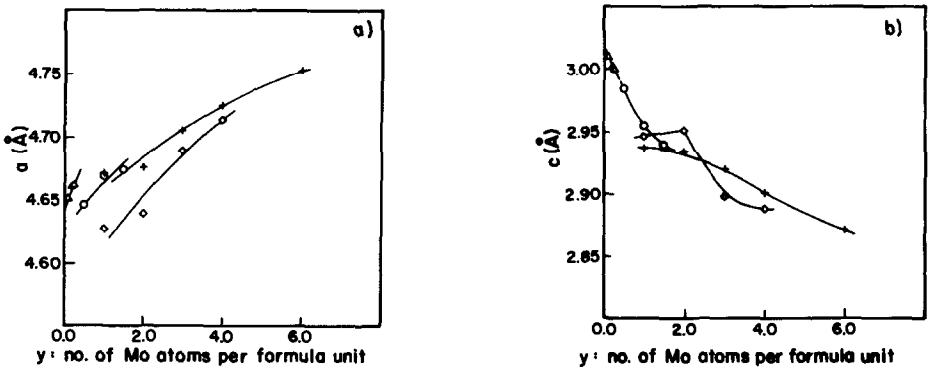

FIG. 3. Variation of the lattice parameters a (a) and c (b) as a function of MoO_2 content in $CrNbO_4$–xVO_2–$yMoO_2$, △, $CrNbO_4$–$yMoO_2$ ($0 \le y < 0.3$); ○, $CrNbO_4$–$0.5VO_2$–$yMoO_2$ ($0 \le y < 2$); ◇, $CrNbO_4$–$2VO_2$–$yMoO_2$ ($0 \le y < 5$); +, $FeNbO_4$–$2VO_2$–$yMoO_2$ ($0 \le y \le 6$).

TABLE I

CRYSTAL DATA FOR MO_2 COMPOUNDS WITH RUTILE-RELATED STRUCTURES

Compound	a (Å)	b (Å)	c (Å)	β (Å)	V (Å)	c/a	Shortest M–M distances (Å)	Ref.
CrO_2	4.4219(5)		2.9162(3)		57.02	0.660	2.92	*3*
VO_2 (tetr)	4.552(1)		2.846(1)		58.97	0.625	2.85	*3*
VO_2 (mon)	5.7517	4.5278	5.3825	122.65	59.00	0.626[a]	2.62	*3*
MoO_2	5.6109(8)	4.8562(6)	5.6285(7)	120.95	65.76	0.577[a]	2.51	*3*
NbO_2	13.690(1)		5.9871(3)		70.13	0.618	2.80	*3*
$V_{0.90}Mo_{0.10}O_2$	4.573		2.860		59.81	0.625	2.860	*5*
$V_{0.50}Mo_{0.50}O_2$	4.680		2.854		62.51	0.610	2.854	*5*
$V_{0.30}Mo_{0.70}O_2$	4.747		2.831		63.79	0.596	2.831	*5*
$Cr_{0.33}Mo_{0.67}O_2$	4.696		2.886		63.64	0.614	2.886	*5*
$Cr_{0.22}Mo_{0.78}O_2$	4.749		2.858		64.46	0.602	2.858	*5*
$CrNbO_4$–xVO_2								
$x = 0$	4.635		3.005		64.56	0.648	3.00	*18*
$x = 1$	4.606(2)		2.989(2)		63.43	0.649	2.99	This work
$x = 2$	4.579(2)		2.961(2)		62.09	0.646	2.96	This work
$x = 3$	4.572(2)		2.952(2)		61.71	0.646	2.95	This work
$x = 6$	4.557(2)		2.924(2)		60.71	0.642	2.92	This work
$CrNbO_4$–xVO_2–$yMoO_2$								
$x = 1, y = 1$	4.651(2)		2.951(2)		63.82	0.634	2.95	This work
$x = 1, y = 2$	4.681(2)		2.921(2)		63.99	0.624	2.92	This work
$x = 2, y = 1$	4.628(2)		2.947(2)		63.10	0.637	2.95	This work
$x = 2, y = 2$	4.639(2)		2.951(2)		63.52	0.636	2.95	This work
$x = 2, y = 3$	4.689(2)		2.898(2)		63.72	0.618	2.90	This work
$x = 2, y = 4$	4.713(2)		2.888(2)		64.16	0.613	2.89	This work
$FeNbO_4$–$2VO_2$–$yMoO_2$								
$y = 1$	4.671(2)		2.936(2)		64.08	0.629	2.94	This work
$y = 2$	4.676(2)		2.934(2)		64.15	0.627	2.93	This work
$y = 3$	4.705(2)		2.920(2)		64.64	0.620	2.92	This work
$y = 6$	4.752(2)		2.871(2)		64.83	0.604	2.87	This work

[a] In monoclinic structures: $c/a = a/b + c \sin \beta$ for the rutile pseudocell.

ble I). Analogous data for the simple binary metallic phases of VO_2, MoO_2, NbO_2, semiconducting VO_2, and the $V_{1-x}Mo_xO_2$ metallic ternary phases are included for comparison in Table I. We have mentioned earlier that in ternary phases, such as CrO_2–MoO_2, NbO_2–MoO_2, VO_2–MoO_2, incorporation of molybdenum tends to stabilize the rutile structure and favor metallic behavior (*5, 6*). Further, increasing Mo content results in decreasing values of c/a. In the $CrNbO_4$–xVO_2–$yMoO_2$ (and $FeNbO_4$–$2VO_2$–$yMoO_2$) phases the metal–metal distances (i.e., the c axis) are greater than the critical distance R_c (*2, 25*) necessary for metallic behavior seen by comparing their c/a values with those of known metallic rutiles such as VO_2, MoO_2, and their ternary analogs. Nevertheless, the trend in the axial ratios shows that strong orbital interactions are present and appear to increase with increasing concentrations of molybdenum; these conclusions are also supported by the electrical resistivity and magnetic susceptibility results as will be shown next.

The temperature variation of the resistivity for two representative samples, CrNbV Mo_2O_{10} and $CrNbV_2Mo_3O_{14}$, respectively,

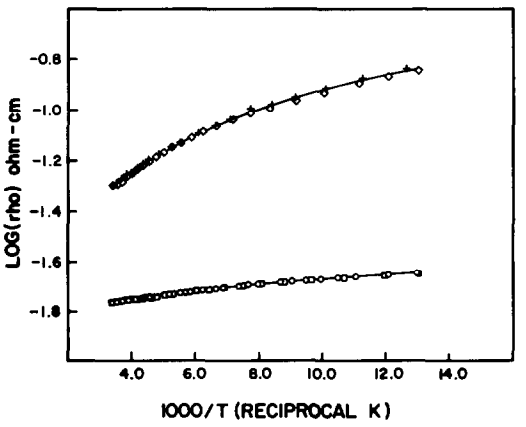

FIG. 4. Temperature variation of the log resistivity of ◇, cooling and +, heating; for $CrNbVMo_2O_{10}$; □, cooling and ○, heating for $CrNbV_2Mo_3O_{14}$.

in the temperature range 77–300 K (Fig. 4) show small band gap semiconducting behavior. The apparent temperature dependence of the activation energy (E_a) of each sample between 77–300 K is likely to be due to a distribution of impurity and/or defect levels that lie in the gap. Room-temperature conductivities and approximate high- and low-temperature limits of E_a for selected samples given in Table II show that the electrical conductivities (σ) increase with increasing molybdenum content, and that the E_a values are very low ($<kT$) for all of the samples.

Why E_a decreases with increasing molybdenum content (Table II) is not clear. It is possible that with increasing Mo content the bottom of the conduction band is lowered, or that the molybdenum source materials contain impurities with very small E_a whose concentration in the sample would increase with increasing Mo content. The temperature variation of resistivity of one of the samples, $CrNbV_2Mo_4O_{16}$, was also studied in the low temperature range 4.2–77 K; no unusual feature in the plot was observed. Qualitative measurement of the sign of the Seebeck coefficient at room temperature indicated that the majority carriers are electrons in all of the $CrNbO_4$–xVO_2–$yMoO_2$ rutile phases studied here.

$FeNbV_2Mo_4O_{16}$ has a lower conductivity σ (300 K) = 76.9 Ω-cm^{-1} than the analogous Cr compound (Table II). However, the Fe compounds are *p*-type semiconductors suggesting that the mechanism of transport in these compounds is different.

It is possible that the observed transport properties are due to localization of the $3d^3$ electrons on the Cr^{3+} ions (as in $Cr^{3+}Nb^{5+}V^{4+}Mo_2^{4+}O_{10}$, for example) which have a very large octahedral crystal field stabilization energy and are unlikely to participate in either M–M σ or M–M π bonding. This would interrupt metallic interactions alone and result in semiconducting behavior of these compounds. Nb^{5+} with no *d* electrons would have a similar interrupting effect on metallic interactions. Finally, the disordered distribution of metal ions with different orbital energies is likely to be a sufficient driving force for semiconducting behavior.

The magnetic susceptibility data of selected samples in the $CrNbO_4$–xVO_2–$yMoO_2$ series are summarized in Table III. The results show that in contrast to the first three samples where both Cr^{3+} and V^{4+} have magnetic moments and contribute to the observed Curie constant, C_m (obtained

TABLE II

ELECTRICAL PROPERTIES OF SELECTED COMPOUNDS IN THE $CrNbO_4$–xVO_2–$yMoO_2$ SYSTEM

Compound	σ (300 K) (Ω-cm^{-1})	E_a (eV) High *T*	E_a (eV) Low *T*
$CrNbVO_6$	1.8×10^{-3}	0.22	—
$CrNbVMoO_8$	3.68 ± 0.02	0.037	0.024
$CrNbVMo_2O_{10}$	19.8 ± 0.1	0.014	0.008
$CrNbV_2MoO_{10}$	2.00 ± 0.02	0.060	0.019
$CrNbV_2Mo_2O_{12}$	1.45 ± 0.01	0.032	0.017
$CrNbV_2Mo_3O_{14}$	58.8 ± 0.8	0.003	0.002
$CrNbV_2Mo_4O_{16}$	148.3 ± 0.8	~0	~0
$FeNbV_2Mo_4O_{16}$	76.9 ± 0.8	0.011	0.007

TABLE III

MAGNETIC DATA FOR SELECTED RUTILE PHASES STUDIED

Compound	Temperature range of Curie-Weiss law fit	C_m(exp)	C_m(theo)[a]	θ
$CrNbO_4$[b]		1.875	1.875	
$CrNbVO_6$[c] ($x = 1, y = 0$)	100–300 K	2.23	2.25	−13
$CrNbV_2O_8$ ($x = 2, y = 0$)		2.82	2.625	
$CrNbMo_{0.1}O_{4.2}$ ($x = 0, y = 0.1$)	50–290 K	1.70	1.98	+32
$CrNbV_{0.5}Mo_{1.5}O_8$ ($x = 0.5, y = 1.5$)	50–300 K	1.65	5.06	+22
$CrNbVMoO_8$ ($x = 1, y = 1$)	30–300 K	1.99	3.25	+19.0
$CrNbVMo_2O_{10}$ ($x = 1, y = 2$)	70–300 K	1.82	4.25	+26.0
$CrNbV_2Mo_3O_{14}$ ($x = 2, y = 3$)	30–300 K	1.839	5.62	+19.0
$CrNbV_2Mo_4O_{16}$ ($x = 2, y = 4$)	30–300 K	1.588	6.62	+13.0
$FeNbV_2Mo_6O_{20}$[d]		~2.03	11.12	
$Li_{3.5}CrNbVMo_2O_{10}$		0.8965		

[a] $C_m(\text{theo}) = \frac{1}{8} g^2[S_{Cr^{3+}}(S_{Cr^{3+}} + 1) + xS_{V^{4+}}(S_{V^{4+}} + 1) + yS_{Mo^{4+}}(S_{Mo^{4+}} + 1)]$; $g = 2.0$, $S_{Cr^{3+}} = \frac{3}{2}$, $S_{V^{4+}} = \frac{1}{2}$, $S_{Mo^{4+}} = 1.0$.

[b] Ref. (*8*).

[c] Ref. (*19*).

[d] $S_{Fe^{3+}} = \frac{5}{2}$ (high spin).

for that region of temperature where the data can be fitted to the Curie-Weiss law), when molybdenum is added to the samples it appears that C_m can be essentially accounted for by the Cr^{3+} magnetic contributions alone (C_m(theo) for $Cr^{3+}(d^3)$ is 1.875; see Table III for calculation of C_m assuming localized spins.). There is no strong evidence in any of these compounds that the molybdenum or vanadium ions make any contribution to the observed magnetic moments. It appears that either the individual ions have even number of electrons which are in singlet states, or that the d electrons are paired in metal–metal bonds. This latter possibility is also supported by the decreasing *M–M* distances (Table I) observed with increasing Mo content which might be explained by Mo–Mo, V–Mo, and V–V interactions occurring, but without long range order (i.e., localized clustering). At very low temperatures (<10 K) the susceptibility appears to saturate for samples with high Mo content (Fig. 5) suggesting the onset of antiferromagnetic ordering consistent with the Weiss constant values obtained (Table III). Similar effects were observed in the magnetic behavior of Cr (*26*), Nb (*27, 28*), and Mo (*29*) doped VO_2. Magnetic data of $V^{4+}Mo^{6+}O_5$ showed that the vanadium ions order antiferromagnetically at ~110 K (*30*).

The large negative deviation of C_m from 1.875 at high molybdenum content ($y > 2$ or $y/x > 2$) suggest that perhaps the Cr^{3+} (and the $Fe^{3+}(d^5)$ in $FeNbV_2Mo_6O_{20}$, Table III) moments are changing; either by their oxidation state or by changes in their crystallographic environment, or that a few vana-

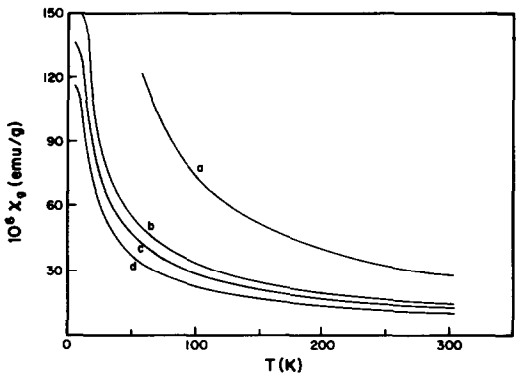

FIG. 5. Temperature variation of the magnetic susceptibility: (a) $CrNbV_2O_8$; (b) $CrNbV_{0.5}Mo_{1.5}O_8$; (c) $CrNbVMo_2O_{10}$; (d) $CrNbV_2Mo_3O_{14}$.

dium ions have developed a moment that is strongly coupled to the Cr moments with an exchange energy of at least a few hundred degrees.

Chemical lithiations with *n*-BuLi in *n*-hexane was carried out on selected samples of these compounds. Each can accommodate substantial amount of lithium (0.5–0.8 Li^+ per MO_2 unit). Upon lithium insertion, the lattice parameters of the host rutile phases change as seen in Table IV where data for selected compounds are given. Also included in Table IV is the data for a partially delithiated sample ($Li_2CrNbVMo_2O_{10}$) obtained by treatment of the fully lithiated sample ($Li_{3.5}CrNbVMo_2O_{10}$) with a calculated quantity of I_2 in acetonitrile to avoid full re-oxidation. The decreasing trend of the axial ratio (c/a) as a function of increasing Mo content seen in the host compounds is also evident in the lithiated phases. The electrochemical lithiation of $CrNbVMo_2O_{10}$ was carried out using a small galvanic test cell. The plot of open-circuit voltage versus lithium content shown in Fig. 6 indicates formation of a single homogeneous phase upon lithium insertion up to 3.5 Li content. The open circuit potential for a particular value of x was obtained by measuring the voltage of the cell immediately after the appropriate amount of current was allowed to pass through it. The potential of the cell was then measured in 24-hr intervals (for several days if required) until a constant potential, indicative of the equilibrium potential values shown in Fig. 6 was obtained. The mobility of Li ions in these rutile structures is low. These results indicate that the performance of these complex rutile-type mixed oxides as cathode materials in secondary lithium batteries is approximately the same as those of the simple binary dioxides such as VO_2 and MoO_2 (*12*).

TABLE IV

LATTICE PARAMETERS OF THE COMPOUNDS FROM LITHIUM INSERTION STUDY

Compound	a (Å)	c (Å)	V (Å^3)	c/a
$CrNbVMo_2O_{10}$	4.651(1)	2.951(1)	63.82	0.634
$Li_2CrNbVMo_2O_{10}$[a]	4.836(3)	2.875(1)	67.24	0.594
$Li_{3.5}CrNbVMo_2O_{10}$[b]	4.969(2)	2.840(1)	70.12	0.572
$Li_{3.5}CrNbVMo_2O_{10}$[c]	4.966(3)	2.841(2)	70.06	0.572
$CrNbV_2Mo_4O_{16}$	4.713(1)	2.888(1)	64.16	0.613
$Li_{4.8}CrNbV_2Mo_4O_{16}$	4.796(5)	2.861(4)	65.82	0.596
$CrNbMo_{0.25}O_{4.5}$	4.662(1)	3.000(1)	65.20	0.644
$Li_{0.7}CrNbMo_{0.25}O_{4.5}$	4.711(3)	2.988(2)	66.30	0.634

[a] Compound obtained from partial delithiation of $Li_{3.5}CrNbVMo_2O_{10}$ by I_2 in CH_3CN.
[b] Compound obtained from electrochemical lithiation of $CrNbVMo_2O_{10}$.
[c] Compound obtained from full chemical lithiation of $CrNbVMo_2O_{10}$.

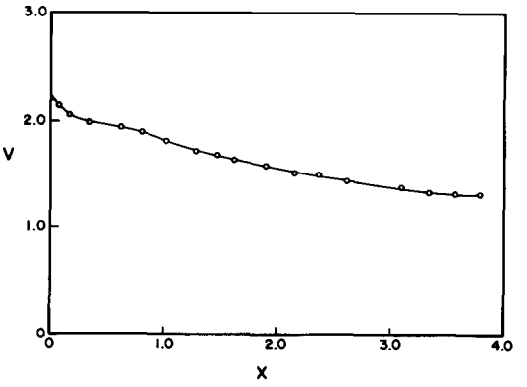

FIG. 6. Open-circuit voltage vs x for Li|1 M $LiClO_4$,PC|$Li_xCrNbVMo_2O_{10}$.

Conclusion

A wide range of solid solutions have been prepared in the $CrNbO_4$–xVO_2–$yMoO_2$ system with the rutile structure. With inclusion of VO_2 increasing amounts of MoO_2 can be incorporated in this system. The metal–metal interactions along the c direction of the rutile structure are enhanced by increasing the Mo content as indicated by the decreasing axial ratios (c/a) and increased magnetic interactions. This may be explained by increased Mo–Mo interactions occurring along the c direction, but without long-range order.

The temperature variation of the electrical conductivity of all the samples shows small band gaps semiconducting behavior, with very small E_a's ($E_a < kT$).

Lithium insertion reactions with n-BuLi and by electrochemical means indicate that substantial amounts of Li can be incorporated in these rutile phases, however, the diffusion rate is very slow.

Acknowledgments

We thank F. J. DiSalvo and W. H. McCarroll for helpful discussions, and K. V. Ramanujachary for technical assistance. Supported by National Science Foundation—Solid State Chemistry Grant DMR-84-04003 (M.G., K.R.N.) and the Office of Naval Research (C.J.C.).

References

1. J. B. GOODENOUGH, "Magnetism and the Chemical Bond," Interscience Monograph on Chemistry, Inorganic Chemistry Section, Vol. 1 (F. A. Cotton, Ed.), Wiley-Interscience, New York/London, 1963.
2. J. B. GOODENOUGH, *Bull. Soc. Chim. France* **4,** 1200 (1965).
3. D. B. ROGERS, R. D. SHANNON, A. W. SLEIGHT, AND J. L. GILLSON, *Inorg. Chem.* **8,** 841 (1969).
4. A. MAGNELI AND G. ANDERSON, *Acta Chem. Scand.* **9,** 1378 (1955).
5. B.-O. MARINDER AND A. MAGNELI, *Acta Chem. Scand.* **12,** 1345 (1958).
6. B.-O. MARINDER AND A. MAGNELI, *Acta Chem. Scand.* **11,** 1635 (1957).
7. B.-O. MARINDER, E. DORM, AND M. SELEBORG, *Acta Chem. Scand.* **16,** 293 (1962).
8. B. KHAZAI, R. KERSHAW, K. DWIGHT, AND A. WOLD, *J. Solid State Chem.* **39,** 395 (1981).
9. B. KHAZAI, R. KERSHAW, K. DWIGHT, AND A. WOLD, *J. Solid State Chem.* **39,** 294 (1981).
10. H. LEIVA, K. DWIGHT, AND A. WOLD, *J. Solid State Chem.* **42,** 41 (1982).
11. P. H. M. DE KORTE, AND G. BLASSE, *J. Solid State Chem.* **44,** 150 (1982).
12. D. W. MURPHY, F. J. DISALVO, J. N. CARIDES, AND J. V. WASZCZAK, *Mat. Res. Bull.* **13,** 1395 (1978).
13. B. G. BRANDT AND A. C. SKAPSKI, *Acta Chem. Scand.* **21,** 661 (1967).
14. J. B. GOODENOUGH, *J. Solid State Chem.* **3,** 490 (1971).
15. T. A. SASAKI AND K. KIUCHI, *Chem. Phys. Lett.* **84,** 356 (1981).
16. T. A. SASAKI, T. SOGA, AND H. ADACHI, *Phys. Status Solidi B* **113,** 647 (1982).
17. C. BLAW, F. LEENHOUTS, F. VAN DER WOUDE, AND G. A. SAWATZKY, *J. Phys. C* **8,** 459 (1975).
18. K. RAVINDRAN NAIR AND M. GREENBLATT, *Mat. Res. Bull.* **17,** 1057 (1982).
19. M. GREENBLATT, K. RAVINDRAN NAIR, W. H. MCCARROLL, AND J. V. WASZCZAK, *Mat. Res. Bull.* **19,** 777 (1984).
20. K. RAVINDRAN NAIR AND M. GREENBLATT, *Mat. Res. Bull.* **18,** 1257 (1983).
21. K. RAVINDRAN NAIR, M. GREENBLATT, AND W. H. MCCARROLL, *Mat. Res. Bull.* **18,** 309 (1983).
22. L. J. VAN DER PAUW, *Philips Res. Rep.* **13,** 1 (1958).
23. F. J. DISALVO AND J. V. WASZCZAK, *Phys. Rev. B* **23,** 457 (1981).
24. R. D. SHANNON, *Acta Crystallogr. Sect. A* **32,** 751 (1976).
25. J. B. GOODENOUGH, *Czech. J. Phys.* **4,** 304 (1967).
26. G. VILLENEUVE, A. BORDET, A. CASALOT, AND P. HAGENMULLER, *Mat. Res. Bull.* **6,** 119 (1971).
27. W. RUDORFF AND T. MARKLIN, *Z. Anorg. Allg. Chem.* **334,** 142 (1964).
28. J. P. POGET, P. LEDERER, D. S. SCHREIBER, H. LAUNOIS, D. WOHLLEBEN, A. CASALOT, AND G. VILLENEUVE, *J. Phys. Chem. Solids* **33,** 1961 (1972).
29. T. HORLIN, T. NIKLEWSKI, AND M. NYGREN, *Mat. Res. Bull.* **8,** 179 (1973).
30. B. BLOM AND M. NYGREN, *Acta Chem. Scand.* **30,** 418 (1976).